Journal of Nuclear Materials 615 (2025) 155945

Contents lists available at ScienceDirect

Journal of Nuclear Materials

journal homepage: www.elsevier.com/locate/jnucmat

Impact of anisotropic grain microstructure on the fracture-mechanical properties of ITER grade tungsten plate

E. Gaganidze *, N. Meena, L. Chauhan, Q. Yuan, J. Aktaa

Karlsruhe Institute of Technology (KIT), Institute for Applied Materials, Hermann-von-Helmholtz-Platz 1, 76344 Eggenstein-Leopoldshafen, Germany

HIGHLIGHTS

- Substantial influence of anisotropic grain microstructure on the fracture behavior
- Moderate scatter of the fracture toughness in the transition region
- Good batch-to-batch reproducibility of fracture-mechanical properties

ARTICLE INFO

Keywords:
ITER grade tungsten
Fracture-toughness
Fracture mode

ABSTRACT

The fracture-mechanical behavior of a uniaxially rolled ITER grade tungsten plate has been investigated up to test temperatures of 700°C. To study the influence of the anisotropic grain microstructure on the Ductile-to-Brittle Transition Temperature (DBTT) and failure mechanism, fracture toughness testing has been performed for four specimen extraction orientations: longitudinal - long transverse (L-T), long transverse - longitudinal (T-L), longitudinal - short transverse (L-S) and long transverse - short transverse (T-S). The DBTTs were at around 250°C and 300°C in L-T and T-L orientations, respectively. In the case of L-S and T-S orientations, the crack deflection prevented unambiguous identification of the DBTT. An upper bound of the DBTT for L-S and T-S orientations was estimated in the range of 300-350°C. Transgranular cleavage was a dominant fracture mode for L-T and T-L orientations at low test temperatures. In contrast to this, for L-S and T-S orientations strong deflections of the crack towards the rolling direction have been recognized which are linked to the anisotropic grain microstructure of the plate material. At the highest test temperatures, no failure of the specimens has been observed up to severe deflection levels which is linked to an extended blunting of the crack starter notch tip and related suppression of the crack initiation and propagation.

1. Introduction

Availability of qualified structural, heat sink and armor materials for the in-vessel components of the future DEMOnstration fusion power plant (DEMO) is a key prerequisite for the realization of DEMO [1]. Severe operational conditions for the DEMO divertor component, designed to exhaust the fusion reaction product helium and impurities, as well as to handle high heat fluxes of up to 10 MW/m^2 during normal operation and up to 20-40 MW/m^2 during slow transient events [2], substantially limit a list of potential materials for Plasma Facing Components (PFCs). Tungsten, owing to a high threshold energy for sputtering by hydrogen isotopes (~ 100-200 eV), a low retention of tritium, a high melting point and a high thermal conductivity, is considered as a baseline armor material for DEMO PFCs [3,4].

A low inherent fracture toughness combined with its relatively high DBTT is, however, a concern for the application of tungsten in PFCs [5–8]. Furthermore, the fabrication-specific anisotropic microstructure is found to have a strong influence on the low-temperature toughness and the DBTT of the polycrystalline tungsten alloys [5,7,9]. The DBTT and toughness are found to be further degraded after neutron irradiation due to alteration of microstructure as a result of the displacement damage and transmutation [10,11]. Full characterization of thermo-physical, mechanical, fracture-mechanical properties, as well as the investigation of high heat-flux and recrystallization behavior, will be required both in the reference unirradiated state as well as after neutron irradiation to enable assessment of the lifetime of DEMO PFCs.

* Corresponding author.
E-mail address: ermile.gaganidze@kit.edu (E. Gaganidze).

https://doi.org/10.1016/j.jnucmat.2025.155945
Received 12 March 2025; Received in revised form 5 May 2025; Accepted 1 June 2025
Available online 2 June 2025

Table 1
ITER specification for chemical elements [13] and the results of manufacturer inspection in wt%.

Elements	W	C	O	N	Fe	Ni	Si
ITER specification	≥ 99.94	≤ 0.01	≤ 0.01	≤ 0.01	≤ 0.01	≤ 0.01	≤ 0.01
Manufacturer inspection	99.99	< 0.001	< 0.001	< 0.001	0.0004	0.0001	< 0.0005

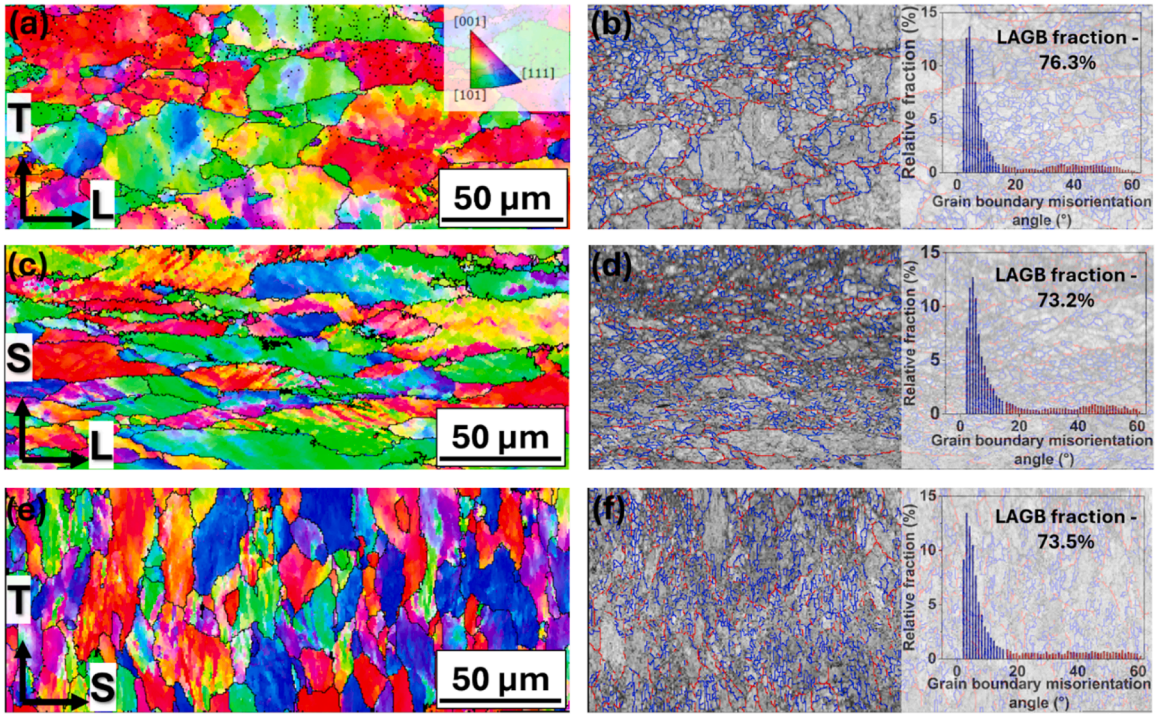

Fig. 1. (a, c, e) illustrate the Inverse Pole Figure (IPF) associated with three distinct planes of the A.L.M.T. tungsten plate, wherein the black lines signify HAGBs (grain misorientation >15°), and (b, d, f) represent the corresponding image quality (IQ) maps associated with T-L, S-L, and T-S orientations, respectively, with the overlap of grain boundaries; the blue lines indicate LAGBs (grain misorientation 2°-15°), while the red lines denote the HAGBs; the inset embedded within the IQ maps elucidates the distribution of grain boundary misorientations.

The main objective of the current work is to study the fracture-mechanical behavior of ITER grade commercial tungsten plate in four different specimen orientations to investigate the influence of fabrication-specific anisotropic microstructure on the fracture toughness and on the failure mechanism. Another objective of this work is to enlarge the fracture toughness database on the ITER specification conform tungsten materials.

2. Experimental

The material studied in the current work was ITER grade tungsten produced by A.L.M.T. Corporation [12] with a lot number PFW-886. The

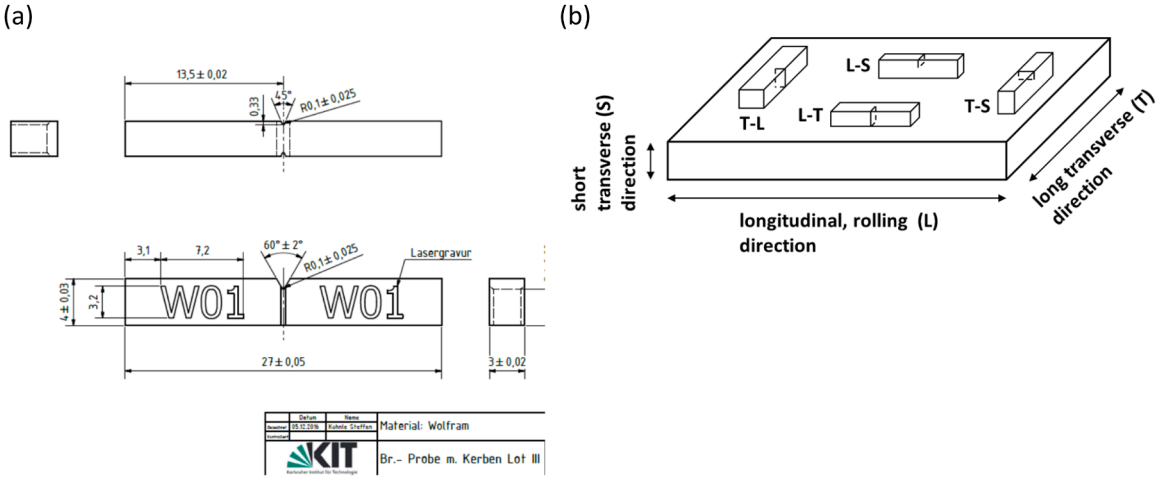

Fig. 2. (a) KLST specimen geometry used for three-point bend fracture-mechanical experiments. (b) Specimen machining directions and specimen crack plane orientations regarding to uniaxially rolled tungsten plate.

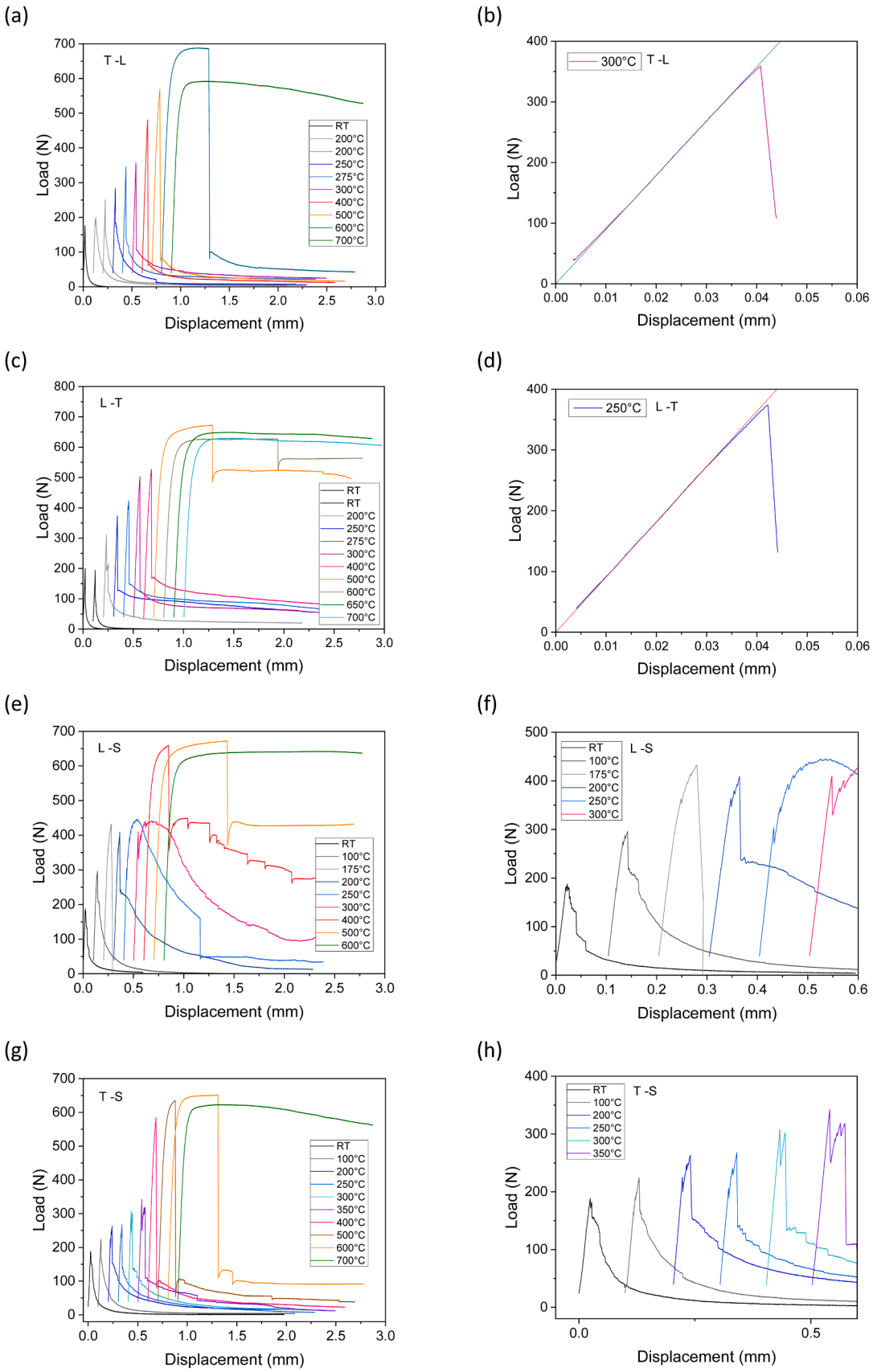

Fig. 3. Load vs. displacement curves in T-L (a),(b); L-T (c),(d); L-S (e),(f) and T-S (g),(h) orientations. For better visualization, the displacement is offset along the x-axis. (b) and (d) magnify the onset of non-linear load vs. displacement behavior for T-L and L-T orientations, respectively. (f) and (h) magnify low T behavior in L-S (e) and T-S (g) orientations, respectively.

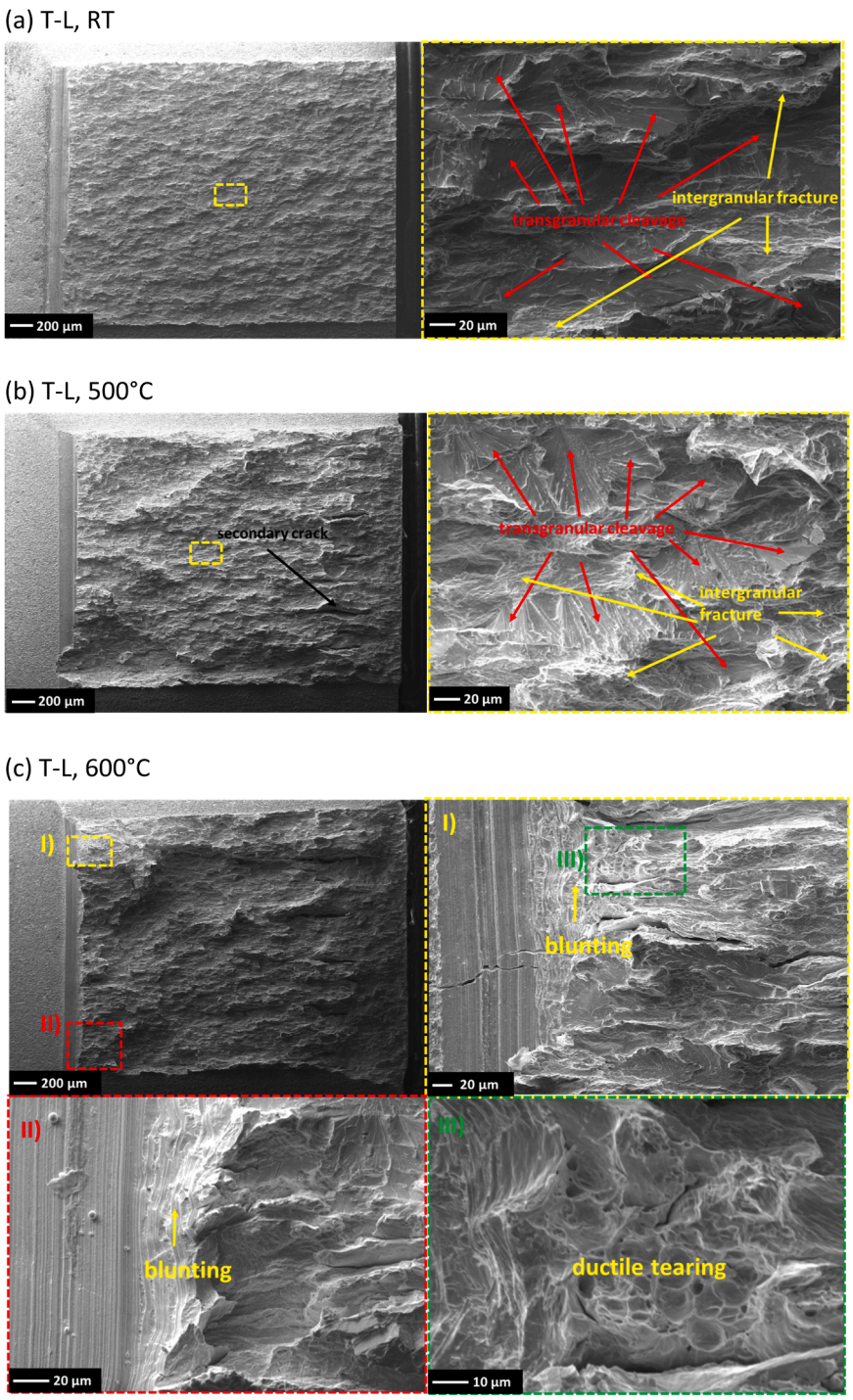

Fig. 4. SEM micrographs of fracture surfaces of selected T-L oriented specimens. The crack propagation direction is from left to right. The magnified areas are marked with a dashed contour of representative color.

main requirements imposed by ITER are summarized in [13]. The requirements on the trace elements were proved to be fulfilled by the manufacturer, see Table 1. The density of 19.24 g/cm^3, minimum hardness (Vickers HV30) of 440, and ASTM grain size number G of 6.5~7.0 were found to comply with the ITER requirements [13] as well. The plate has been delivered in the stress relieved state.

Specimens for initial microstructural characterization were first mechanically polished and then chemically polished with an oxide particle suspension (OPS). Finally, the samples were electropolished with 1.5% NaOH solution at 20 V. The investigation of the microstructure is performed using a Zeiss Evo 10 scanning electron microscope (SEM) equipped with a Bruker e$^-$Flash^{HR} electron backscattered diffraction (EBSD) detector. EBSD data acquisition was performed using an acceleration voltage of 20 kV and 1.7 nA probe current with a step size of 600 nm. Misorientations between 2°-15° were considered as low-angle grain boundaries (LAGBs), whereas misorientations exceeding 15° were considered as high-angle grain boundaries (HAGBs) [14]. EBSD investigations of the plate in all three orthogonal directions have been carried out to get insight into the grain shape, orientation and size. We follow international convention for longitudinal (L), long transverse (T) and short transverse (S) directions of the plate. Inverse Pole Figure (IPF) for T-L, S-L and T-S planes shown in Figure 1 reveals anisotropic grain

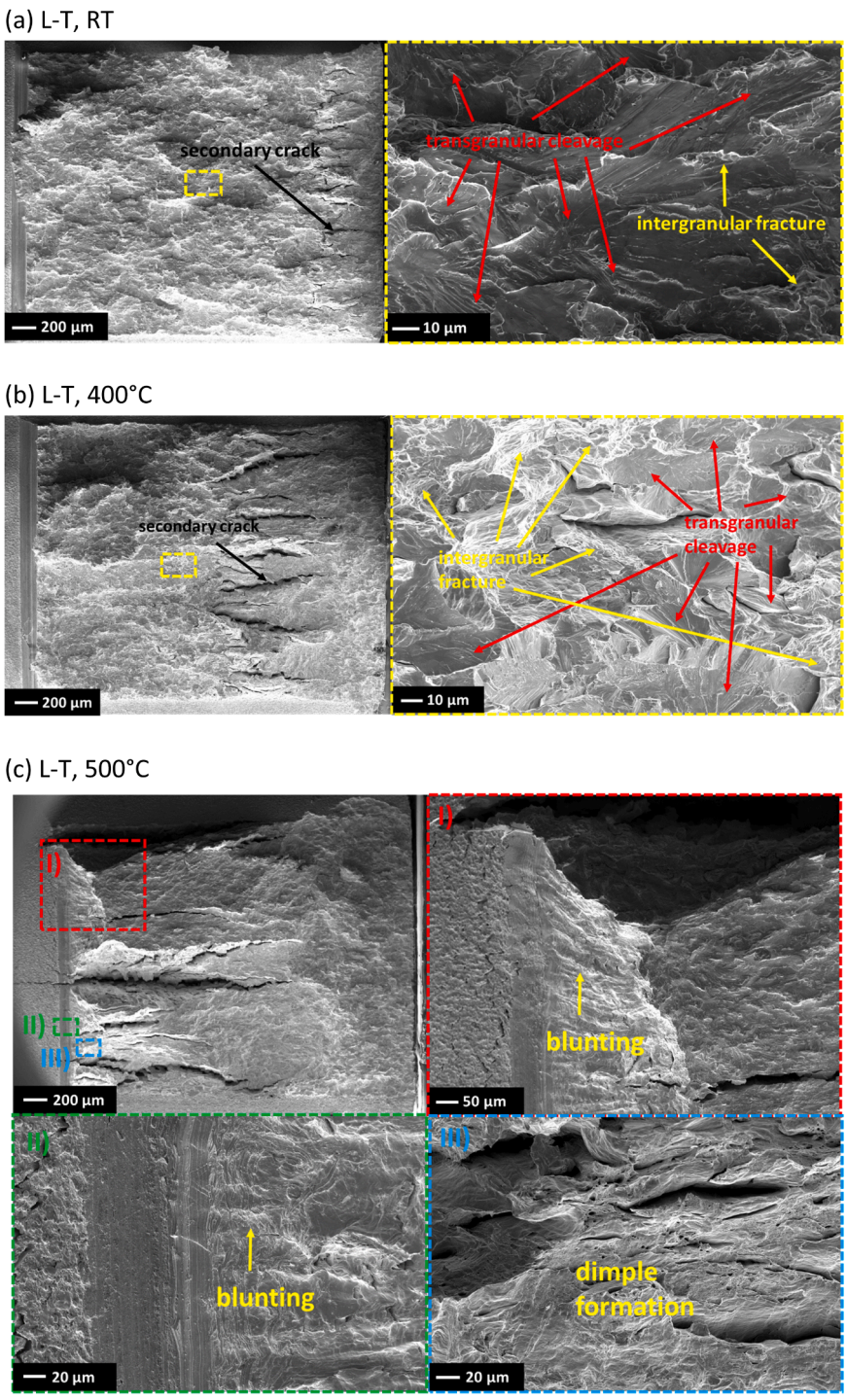

Fig. 5. SEM micrographs of fracture surfaces of L-T oriented specimens. The crack propagation direction is from left to right. The magnified areas are marked with a dashed contour of representative color. The specimen tested at 500°C was broken after test at RT for SEM examination purpose.

microstructure with elongated grains in the rolling direction (L). Furthermore, examining the grain misorientation distributions for these orientations, see Figure 1(b),(d),(f), indicates that the LAGBs proportion across the T-L plane is comparatively higher in relation to the other two perpendicular planes, namely S-L and T-S. The average grain sizes, determined by applying the line-intercept method by considering grains with misorientation angles >15° were found to be about 20.0, 12.5 and 10.0 µm for T-L, S-L and T-S planes, respectively. This correlates with a higher fraction of LAGBs in the T-L plane.

Fracture-mechanical three-point bend (3PB) specimens of KLST type with the dimensions Thickness (B) x Width (W) x Length (L) of 3 × 4 × 27 mm^3, and a 1 mm deep V-type notch, see Fig. 2(a), were fabricated by Electrical Discharge Machining (EDM) in T-L, L-T, L-S and T-S orientations as shown schematically in Fig. 2(b). The reader is also referred to [15] for orientation of the specimens. To increase the stress triaxiality, sharp, crack starter notches have been introduced by razor blade polishing. The average notch diameter of 45.8 µm (SD = 9.6 µm) and an average initial crack length (a_0) of 1.193 mm have been achieved. Finally, side grooves of ca. 0.33 mm depth for each side were introduced according to Fig. 2(a) leading to a reduction of nominal net thickness

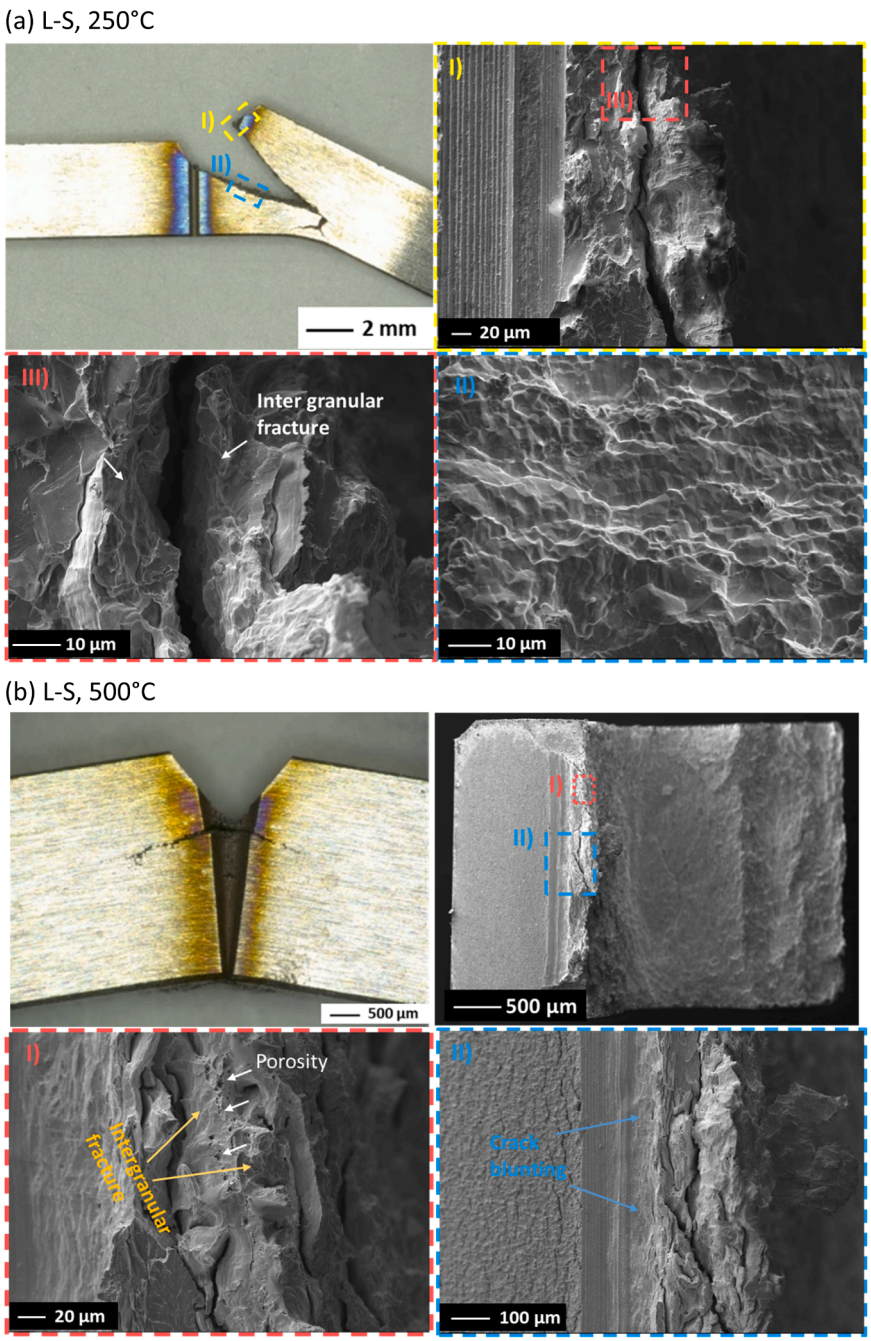

Fig. 6. Optical images and SEM micrographs of fracture surfaces of selected L-S oriented specimens. The crack propagation direction is from left to right in the SEM images. The magnified areas are marked with a dashed contour of representative color. In the case of (b) specimen was broken after cooling down at RT.

(B_N) down to 2.34 mm. The quasi-static 3PB experiments were carried out following ASTM E399 [15] aiming to determine the plane strain fracture toughness K_{Ic}. The distance S between the specimen support pins during the 3PB tests was 25 mm. The applied deflection rate of 2 µm/s resulted in stress intensity factor rates between 0.7-0.9 MPa·$m^{1/2}$/s. Tests were performed with an INSTRON-DOLI universal electromechanical testing machine equipped with a high-temperature vacuum furnace (up to 1500°C). The room temperature (RT) tests were carried out under an ambient atmosphere, and the high-temperature tests were performed under a typical vacuum of 10^{-5} mbar. SEM (scanning electron microscopy) examinations of the fracture surfaces of broken specimens were performed with a Zeiss EVO MA 10 SEM.

3. Results

The recorded load vs. displacement curves are summarized in Fig. 3 for all investigated orientations. Fig. 3(a) shows the results for T-L orientation. Up to 275°C specimens failed in a brittle manner without inelastic deformation. The first sign of non-linear behavior in the load displacement curve was registered at 300°C, see the magnified curve in Fig. 3(b). With increasing the tests temperature, the amount of inelastic deformation prior to unstable crack initiation/propagation was increased. The increase of the amount of inelastic deformation and maximum loads achieved prior to fracture with increasing the temperature reflects the increase of the toughness of the material. The initiation of brittle crack has not been suppressed up to a test temperature of 600°C. Testing at 700°C in contrast revealed full suppression of the crack

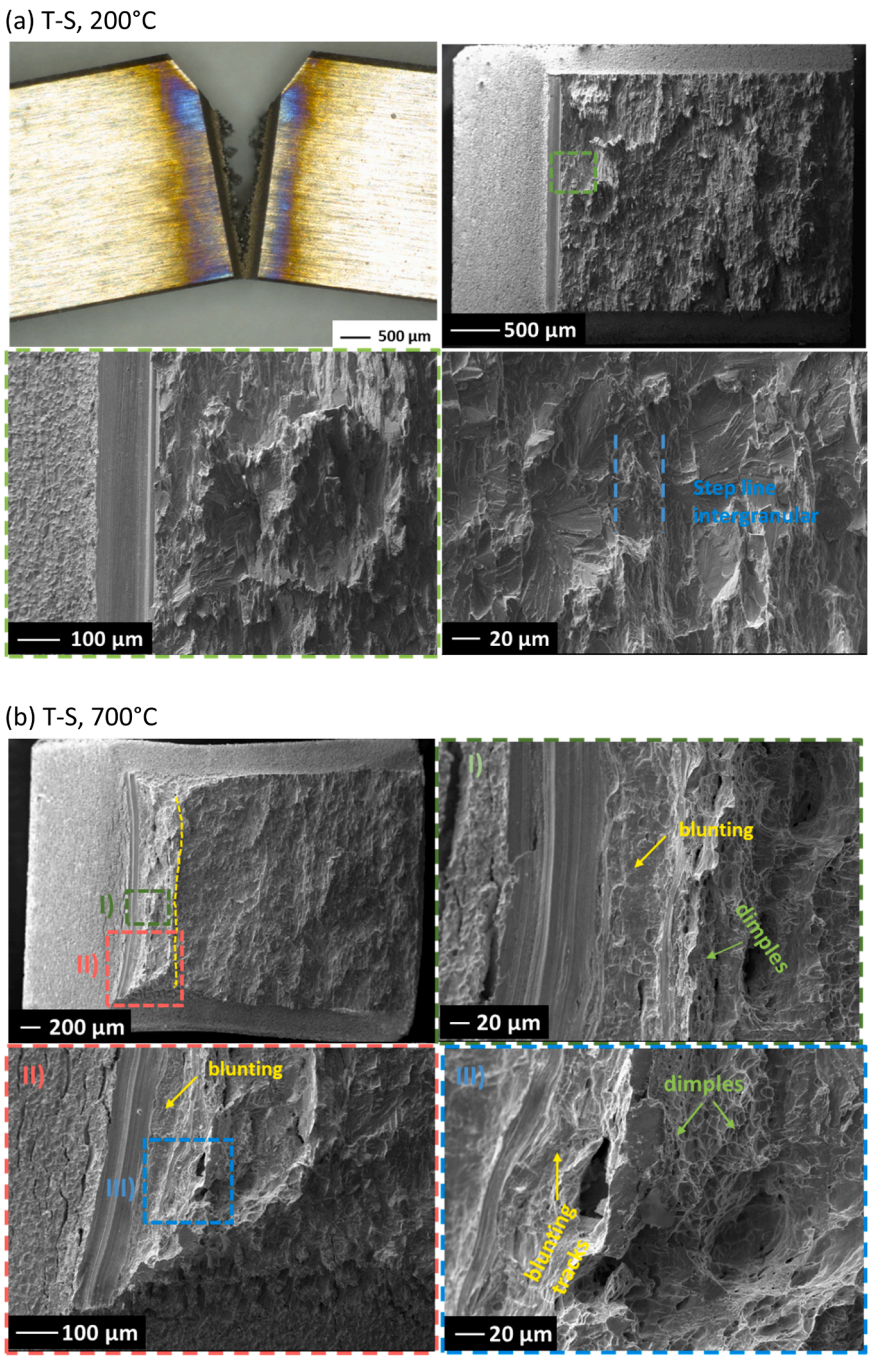

Fig. 7. Optical image and SEM micrographs of fracture surfaces of selected T-S oriented specimens. The crack propagation direction is from left to right in the SEM micrographs. The magnified areas are marked with a dashed contour of representative color. The yellow dotted line in (b) marks a crack front. Here the specimen was broken after high temperature test at RT for SEM examination purpose.

initiation, which is attributed to an extended blunting of the crack starter notch, see Fig. 4(c).

The load vs. displacement curves in L-T orientation are shown in Fig. 3(c). Up to 200°C specimens failed in a brittle manner without inelastic deformation. The first sign of non-linear behavior in the load displacement dependence was observed at 250°C, see the magnified curve in Fig. 3(d). This temperature is by 50°C lower than the corresponding one in T-L orientation. With further increasing the test temperature, the amount of inelastic deformation prior to initiation and propagation of unstable crack has been increased. Testing at 500°C and above revealed crack initiation and arrest events manifested as sudden partial load drops. At a test temperature of 650°C, a full suppression of unstable crack propagation was observed due to extended blunting of the specimen, see Fig. 5(c).

The load vs. displacement curves obtained in L-S orientation are shown in Fig. 3 (e)(f). Onset of nonlinearity in the curves is observed already at very low test temperatures due to crack deflection tendency towards the rolling direction (see Fig. 6(a)), which is attributed to the anisotropic grain microstructure shown in Fig. 1. Due to such behavior, in contrast to T-L and L-T orientations, the DBTT cannot be clearly defined, as the onset of the nonlinearity does not evince onset of the ductile behavior. Multiple crack initiation and arrest events take place up to 500°C. Finally, at a test temperature of 600°C full suppression of the crack propagation is observed.

The load vs. displacement curves obtained in T-S orientation are shown in Fig. 3 (g)(h). Similar to the L-S orientation, the onset of nonlinearity in the curves takes place at very low test temperatures. The crack propagation appears to follow a zig-zag like path as shown in Fig. 7 (a) with lesser amount of deflections towards the rolling direction as compared with L-S orientation observed in Fig. 6(a). Also, in this case, the determination of the DBTT from the load vs. displacement curves is not unambiguous. Testing at 700°C leads to a full suppression of the crack propagation.

Representative SEM micrographs of fracture surfaces, together with selected optical images of the tested specimens, are shown in Fig. 4 to Fig. 7. Up to a test temperature of 500°C no macroscopic signs of deformation are revealed for T-L oriented specimens, see Fig. 4(a),(b). The fracture mode is a mixture of transgranular cleavage and intergranular fracture, the former being the dominant mechanism. Formation of secondary cracking transverse to the main crack plane is observed in addition at 500°C. At 600°C the deformation and fracture behavior are substantially modified, see Fig. 4(c). This is manifested in the formation of an extensive blunting zone prior to the initiation of brittle crack. Moreover, next to the blunting zone and in the vicinity of the necking area dimple formation is observed indicating, ductile tearing of the material. Despite of such initial deformation and fracture behavior, the material loses its load bearing capability and fails in a brittle way as seen in Fig. 3(a).

For the L-T orientation no macroscopic sign of deformation is revealed up to a test temperature of 400°C, see Fig. 5(a)(b). Brittle transgranular cleavage dominates in the examined L-T orientation. Nevertheless, isolated areas of intergranular fracture are observed as well. Fraction of intergranular areas is somewhat lower in the L-T orientation compared to the T-L orientation. Secondary cracks appearing transverse to the main crack plane are observed in L-T orientation as well and their extensions are increased with increasing the temperature. Such a behavior can be presumably attributed to a deflection of crack to follow a weaker intergranular path. The testing at and above 500°C substantially modifies deformation and fracture behavior. Strongly pronounced necking and extended blunting zone developments are observed in Fig. 5(c). Furthermore, severe secondary cracking formation is seen. Remarkably, the orientation of secondary cracks with respect to the main crack plane varies, presumably due to variation in the local grain microstructure. In the vicinity of the secondary cracking, the onset of ductile dimple formation, being characteristic to ductile tearing is registered at these elevated temperatures. Formation of secondary cracking is frequently observed in the case of uniaxially rolled material when tested in 'strong' orientation, see e.g. [16]. Comparatively, fracture behavior was fully brittle in the case of T-L orientation at 500°C indicating major differences between T-L and L-T orientations.

A severe deflection of the crack has been observed after testing the L-S oriented specimen at and above 200°C, see exemplarily the fracture behavior at 250°C in Fig. 6(a). SEM micrographs of fracture surface identifies propagation of a secondary crack transverse to the main crack plane in the vicinity of the notch, see red dashed box in Fig. 6(a). A closer look into the crack opening reveals intergranular fracture mode. Fracture mode of the deflected crack far from the initial crack notch is intergranular as well, see the blue box in Fig. 6(a). Testing at 500°C in L-S orientation resulted pure delamination of the material, as seen in Fig. 6 (b). For SEM investigation, the specimen was cooled down to RT and broken in a brittle way. Formation of the secondary cracks leading to the delamination of the material is seen in red box of Fig. 6(b). Traces of intergranular fracture regions and formation of the deformation-induced pores are revealed in the vicinity of the secondary cracks. The presence of pores may indicate an onset of dimple formation even though the dimples are not fully developed. Furthermore, formation of the extended blunting is identified next to the initial notch front.

A zig-zag like crack propagation is seen for T-S orientation at a test temperature of 200°C, see optical image in Fig. 7(a). SEM micrograph of overall fracture surface reveals uneven, brittle fracture behavior.

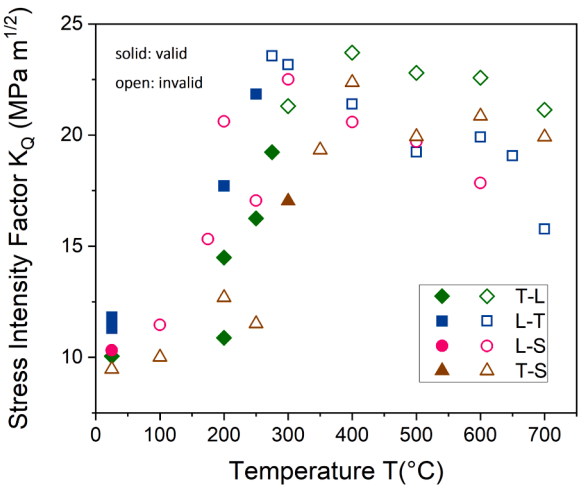

Fig. 8. Fracture toughness vs. test temperature of A.L.M.T. W plate for four investigated orientations. Values represented by open symbols do not satisfy the ASTM 399 validity criteria; see text. dK/dt = 0.7- 0.9 MPa m$^{1/2}$ /s.

Alternation of dominant transgranular cleavage (expected for the T-S orientation) and step line intergranular fracture areas, see marking in Fig. 7(a), confirms the observed zig-zag like crack propagation revealed by an optical image. Testing at 700°C did not lead to the propagation of the crack in a good agreement with the corresponding load vs. displacement curve in Fig. 3(g). For subsequent SEM investigations shown in Fig. 7(b) the specimen was broken by a brittle fracture after cooling down to RT. An extended blunting zone are observed next to the initial crack front. Furthermore, the onset of extensive dimple formation is seen in the necking area of the specimen.

4. Discussion

Conditional values of fracture toughness (K_Q) have been calculated according to ASTM E399 procedure following the stress intensity factor equation for 3PB specimens

$$K_Q = \frac{P_Q S}{\sqrt{B B_N} W^{3/2}} f\left(\frac{a}{W}\right).$$

Here the conditional load P_Q is determined from the load-displacement curves via constructing the secant line through the origin of the test record with a slope equal to 95% of the slope of the initial linear portion. The geometry factor $f(a/W)$ for 3PB specimens is calculated according to ASTM E399 [15]. Specimen load bearing capability $P_m/P_Q \leq 1.1$ (with P_m being the maximum load) and the requirement on the small scale yielding $2.5(K_Q/\sigma_{YS})^2 < W\text{-}a_o$ have been examined to qualify K_Q as valid K_{Ic} in the framework of linear-elastic fracture-mechanics. Approximate values of yield strength (σ_{YS}) have been used from the literature [17,18] for this purpose.

The fracture toughness values obtained in all four orientations are summarized in Fig. 8. The results satisfying the validity criteria are shown with solid symbols while the invalid results are represented with open ones. In the case of T-L and L-T orientations steep increases of the valid fracture toughness values are observed above 200-250°C. The DBTTs of 300 and 250°C are identified on the base of the onset of nonlinearities in the load vs. displacement curves (Fig. 3) for T-L and L-T orientations, respectively. It is worth noting that the DBTT determined via identification of the temperature for the appearance of the first sign of non-linearity in the load vs. displacement curves was found to agree well with the DBTT determined on the base of application of 5% flexural strain criteria and appeared to correlate with a steep increase of the fracture toughness, see e.g. [10]. Higher DBTT for the *weak* orientation with expected crack propagation direction along the elongated grains

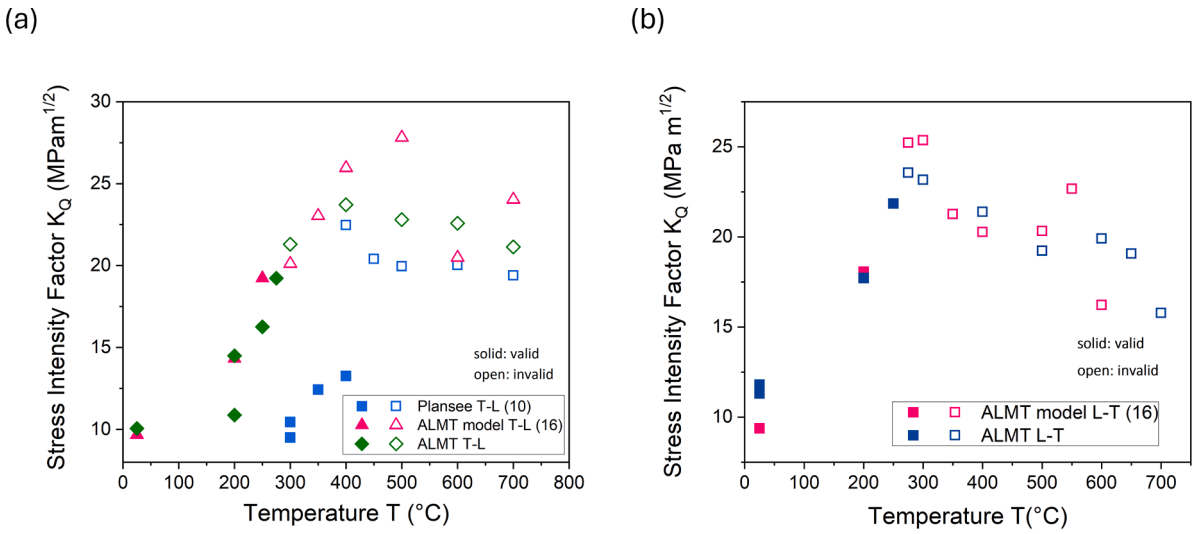

Fig. 9. Fracture toughness of different ITER specification confirm grades for T-L and L-T orientations. The results on Plansee forged bar are from [10] and the results on A.L.M.T. model plate stem from [16].

are typically observed for different rolled or forged polycrystalline tungsten products [5,7,9]. This was primarily explained by the dominance of intergranular fracture mode. In the current study the dominant fracture mode is the transgranular cleavage even in the *weak* T-L orientation. Similar observations have been observed in more recent studies on ITER grade tungsten products such as forged tungsten bar from Plansee [11] and rolled model plate from A.L.M.T [16]. Such observation can be interpreted as substantial improvement of grain boundary cohesion which can be partly attributed to stronger control of the trace elements in ITER grade W products. The presence of impurities, such as phosphor was found responsible for intergranular fracture in [19]. In technically pure (99.97% purity) tungsten detailed investigation of effect of representative impurities (P, O, S) revealed that small amount of impurities do not influence the crack path, while other factors e.g. grain microstructure and dislocation density were found to have a stronger influence on fracture mechanisms [20]. In spite of the fact that transgranular cleavage was dominant fracture mode both in T-L and L-T orientations the fraction of transgranular cleavage appeared to be somewhat higher in the L-T orientation. Arrangement of the elongated grains transverse to the main crack plane, as revealed in Fig. 1, explains slightly higher fracture toughness and lower DBTT in the L-T orientation compared to T-L orientation.

The nonlinearities observed in the load vs. displacement curves for L-S and T-S orientations even at low test temperatures prevented the determination of valid fracture toughness values in the transition region and the identification of the DBTT as the temperature for the onset of the nonlinearity. The observed crack deflections are related to the strongly anisotropic grain microstructure as shown in Fig. 1. Lower intergranular fracture energy compared to the fracture energy of the bulk (matrix) material is believed to be responsible for the observed crack deflection phenomena [5]. Based on the moderate scatter of the toughness data in the transition region with the results in the L-S and T-S orientations building the left and right bounds of the scatter band, the DBTTs can be confined between 250 and 350°C irrespective of the orientation. Though anisotropic grain microstructure was found to substantially affect the fracture mechanism, its effect on the DBTT is found to be limited. Nevertheless, the pronounced crack deflection of the crack propagation observed in L-S and T-S orientations favors T-L orientation for the manufacturing of ITER-like divertor components [2]. In-fact the T-L orientation would prevent formation of transverse cracks and thus would avoid interruption of heat-flux flow from monoblock plasma facing surface down to the coolant CuCrZr tube.

The absence of the sharp fatigue pre-crack may affect the measured fracture toughness particularly in the upper shelf. In [21] the influence of different precrack introduction methods, including razor blade polishing and compression fatigue pre-cracking, on the measured fracture toughness has been examined. Notch diameters of about 40 μm have been achieved by applying the razor blade polishing technique. For L-R orientation at RT the fracture toughness measured on compression fatigue pre-cracked specimens was scattered between 12-14 MPam$^{1/2}$, whereas fracture toughness of about 14 MPam$^{1/2}$ was reported on the specimen with a notch refined by razor blade polishing. This indicates that even though razor blade polishing tendentially leads to the increase of the fracture toughness its effect below the DBTT is still moderate.

Above about 400°C the conditional toughness values decrease with increasing the temperature for all orientations. Such behavior does not reflect the decrease of the toughness of the material but is rather attributed to the loss of its tensile strength. Strong necking of the specimens and the excessive blunting of the notch tip at elevated temperatures are direct manifestations of the loss of the constraint. The limitation of the application of linear-elastic fracture-mechanics in the ductile regime can be overcome by applying elastic-plastic fracture-mechanics concept for the determination of the crack resistance curve behavior according to ASTM E1820 [22]. This would however require the use of larger fracture-mechanical specimens and implementation of the fatigue pre-cracking instead of using the razor blade polishing in order to achieve high triaxiality stress state to suppress severe blunting of the crack tip.

Fracture toughness results obtained in the current work on commercial A.L.M.T. plate are compared to those of different ITER specification conform products for T-L and L-T orientations in Fig. 9. Fracture-mechanical properties of ITER grade commercial tungsten plate resemble for both orientations to those of ITER specification conform uniaxially rolled model plate from A.L.M.T. studied in [16]. This observation proves good batch-to-batch reproducibility of the ITER specification conform A.L.M.T. tungsten plates. Batch-to-batch reproducibility is one of the main requirements for the unambiguous determination of design limit data enabling safe design of the components. Furthermore, as already found in [16] the fracture-mechanical performance of the A.L.M.T. rolled plate is confirmed to show superior behavior over the ITER specification conform Plansee forged bar studied in [10]. The DBTT of the A.L.M.T. plate is at least 100°C lower than the DBTT of the Plansee bar in the weakest T-L orientation.

5. Summary

Fracture-mechanical behavior of ITER specification-conform tungsten plate commercially produced by A.L.M.T., Japan, has been investigated up to test temperatures of 700°C. The quasi-static fracture-mechanical experiments were carried out following ASTM E399 to determine plane strain fracture toughness K_{Ic}. Deformation and fracture mechanisms have been studied by employing optical and SEM investigations. Fracture mode was predominantly transgranular for T-L and L-T orientations, even though somewhat higher fraction of intergranular fracture was observed in T-L orientation compared to L-T one. In contrast to this, for L-S and T-S orientations strong deflections of the crack towards the rolling direction have been recognized, which are linked to the anisotropic grain microstructure of the plate material. Though anisotropic grain microstructure was found to substantially affect the fracture mechanism, its effect on the DBTT is found to be limited. Taking into account the overall moderate scatter of the fracture toughness data in the transition region, the DBTTs between 250 and 350°C have been identified. At the highest test temperatures, no failure of the specimens up to severe deflection levels has been observed which is linked to an extended blunting of the crack starter notch tip and related suppression of the crack initiation and propagation. Good batch-to-batch reproducibility of fracture-mechanical properties has been concluded for ITER specification conform A.L.M.T. tungsten plates.

CRediT authorship contribution statement

E. Gaganidze: Writing – original draft, Methodology, Investigation, Conceptualization. **N. Meena:** Writing – review & editing, Investigation. **L. Chauhan:** Writing – review & editing, Investigation. **Q. Yuan:** Writing – review & editing, Investigation. **J. Aktaa:** Writing – review & editing, Resources.

Declaration of competing interest

The authors declare that they have no known competing financial interests or personal relationships that could have appeared to influence the work reported in this paper.

Acknowledgement

This work has been carried out within the framework of the EUROfusion Consortium, funded by the European Union via the Euratom Research and Training Programme (Grant Agreement No 101052200 — EUROfusion). Views and opinions expressed are however those of the author(s) only and do not necessarily reflect those of the European Union or the European Commission. Neither the European Union nor the European Commission can be held responsible for them. We kindly acknowledge M. Blem for her support in performing the fracture-mechanical 3PB tests.

Data availability

The authors do not have permission to share data.

References

[1] G. Federici, C. Bachmann, W. Biel, L. Boccaccini, S. Ciattaglia, F. Cismondi, et al., Overview of the design approach and prioritization of R&D activities towards an EU DEMO, Fus. Eng. Design 109-111 (2016) 1464–1474.
[2] J.H. You, E. Visca, T. Barrett, B. Böswirth, F. Gescenzi, F. Domptail, et al., High-heat-flux technologies for the European demo divertor targets: State-of-the-art and a review of the latest testing campaign, J. Nucl. Mater. 544 (2021) 152670.
[3] H. Bolt, V. Barabash, W. Krauss, J. Linke, R. Neu, S. Suzuki, et al., Materials for the plasma-facing components of fusion reactors, J. Nucl. Mater. 329-333 (2004) 66–73.
[4] G. Pintsuk, G. Aiello, S.L. Dudarev, M. Gorley, J. Henry, M. Richou, et al., Materials for in-vessel components, Fus. Eng. Design 174 (2022) 112994.
[5] D. Rupp, S.M. Weygand, Anisotropic fracture behaviour and brittle-to-ductile transition of polycrystalline tungsten, Philos. Mag. 90 (2010) 4055–4069.
[6] B. Gludovatz, S. Wurster, A. Hoffmann, R. Pippan, Fracture toughness of polycrystalline tungsten alloys, Int. J. Refract. Met. Hard Mater. 28 (2010) 674–678.
[7] E. Gaganidze, D. Rupp, J. Aktaa, Fracture behaviour of polycrystalline tungsten, J. Nucl. Mater. 446 (2014) 240–245.
[8] S. Nogami, A. Hasegawa, M. Fukuda, M. Rieth, J. Reiser, G. Pintsuk, Mechanical properties of tungsten: Recent research on modified tungsten materials in Japan, J. Nucl. Mater. 543 (2021) 152506.
[9] M. Conte, J. Aktaa, Manufacturing influences on microstructure and fracture mechanical properties of polycrystalline tungsten, Nucl. Mater. Energy 21 (2019) 100591.
[10] E. Gaganidze, A. Chauhan, H.-C. Schneider, D. Terentyev, G. Borghmans, J. Aktaa, Fracture-mechanical properties of neutron irradiated ITER specification tungsten, J. Nucl. Mater. 547 (2021) 152761.
[11] E. Gaganidze, A. Chauhan, H.-C. Schneider, D. Terentyev, B. Rossaert, J. Aktaa, Effect of irradiation temperature on the fracture-mechanical behaviour of tungsten irradiated to 1 dpa, J. Nucl. Mater. 556 (2021) 153200.
[12] A.L.M.T. Corporation, 1-11-11, Shiba, Minatok-ku, Tokyo, 105-0014, https://www.allied-material.co.jp/en/.
[13] T. Hirai, S. Panayotis, V. Barabash, C. Amzallag, F. Escourbiac, A. Durocher, et al., Use of tungsten material for the ITER divertor, Nucl. Mater. Energy 9 (2016) 616–622.
[14] K. Wang, D. Ren, X. Zan, L. Luo, X. Zhu, Y. Wu, Recrystallization behavior of pure tungsten hot-rolled with high accumulated strain during annealing at 1250°C-1350°C, Mater. Sci. Eng. A 806 (2021) 140828.
[15] ASTM E399 - 17, "Standard Test Method for Linear-Elastic Plane-Strain Fracture Toughness KIc of Metallic Materials," ASTM International, 100 Barr Harbor Drive, PO Box C700, West Conshohocken, PA 19428-2959. United States, 2017.
[16] E. Gaganidze, A. Chauhan, J. Aktaa, Fracture-mechanical behaviour of ITER grade tungsten subjected to three different rolling processes, Fus. Eng. Design 184 (2022) 113300.
[17] M. Wirtz, I. Uytdenhouwen, V. Barabash, F. Escourbiac, T. Hirai, J. Linke, et al., Material properties and their influence on the behaviour of tungsten as plasma facing material, Nucl. Fusion 57 (2017) 066018.
[18] C. Yin, D. Terentyev, T. Pardoen, A. Bakaeva, R. Petrov, S. Antusch, et al., Tensile properties of baseline and advanced tungsten grades for fusion applications, Int. J. Refract. Met. Hard. Mater 75 (2018) 153–162.
[19] Tran Huu Loi, J.P. Morniroli, M. Gantois, Brittle fracture of polycrystalline tungsten, J. Mater. Sci 20 (1985) 199–206.
[20] B. Gludovatz, S. Wurster, T. Weingärtner, A. Hoffman, R. Pippan, Influence of impurities on fracture behaviour of tungsten, Philos. Mag. 91 (2011) 3006–3020.
[21] D. Rupp, Bruch und Spröd-duktil-Übergang in polykristallinem Wolfram: Einfluss von Mikrostruktur und Lastrate, Karlsruhe Institute of Technology, 2010. PhD thesis.
[22] ASTM E1820 - 18a, "Standard Test Method for Measurement of Fracture Toughness," *ASTM International, 100 Barr Harbor Drive, PO Box C700, West Conshohocken, PA 19428-2959. United States,* 2018.